ACS NANO
Cite This: ACS Nano 2018, 12, 9549–9557
www.acsnano.org

ARTICLE

Ultrasensitive Virion Immunoassay Platform with Dual-Modality Based on a Multifunctional Aggregation-Induced Emission Luminogen

Ling-Hong Xiong,[†,‡,§] Xuewen He,[†,§] Zheng Zhao,[†,§] Ryan T. K. Kwok,[†,§] Yu Xiong,[†,§] Peng Fei Gao,[†,§] Fan Yang,[‡] Yalan Huang,[‡] Herman H.-Y. Sung,[†] Ian D. Williams,[†] Jacky W. Y. Lam,[†,§] Jinquan Cheng,[*,‡] Renli Zhang,[*,‡] and Ben Zhong Tang[*,†,§,∥]

[†]Department of Chemistry, Hong Kong Branch of Chinese National Engineering Research Centre for Tissue Restoration and Reconstruction, Institute for Advanced Study and Division of Life Science, The Hong Kong University of Science and Technology, Clear Water Bay, Kowloon 00852, Hong Kong

[‡]Shenzhen Center for Disease Control and Prevention, Shenzhen 518055, China

[§]HKUST-Shenzhen Research Institute, Shenzhen 518057, China

[∥]NSFC Center for Luminescence from Molecular Aggregates, SCUT-HKUST Joint Research Laboratory, State Key Laboratory of Luminescent Materials and Devices, South China University of Technology, Guangzhou 510640, China

Supporting Information

ABSTRACT: **Sensitive and accurate detection of highly contagious virus is urgently demanded for disease diagnosis and treatment. Herein, based on a multifunctional aggregation-induced emission luminogen (AIEgen), a dual-modality readout immunoassay platform for ultrasensitive detection of viruses has been successfully demonstrated. The platform is relied on virions immunobridged enzymatic hydrolysis of AIEgen, accompanying with the *in situ* formation of highly emissive AIE aggregates and shelling of silver on gold nanoparticles. As a result, robust turn-on fluorescence and naked-eye discernible plasmonic colorimetry composed dual-signal is achieved. By further taking advantage of effective immunomagnetic enrichment, EV71 virions, as an example, can be specifically detected with a limit of detection down to 1.4 copies/μL under fluorescence modality. Additionally, semiquantitative discerning of EV71 virions is realized in a broad range from 1.3 × 10^3 to 2.5 × 10^6 copies/μL with the naked eye. Most importantly, EV71 virions in 24 real clinical samples are successfully diagnosed with 100% accuracy. Comparing to the gold standard polymerase chain reaction (PCR) assay, our immunoassay platform do not need complicated sample pretreatment and expensive instruments. This dual-modality strategy builds a good capability for both colorimetry based convenient preliminary screening and fluorescence based accurate diagnosis of suspect infections in virus-stricken areas.**

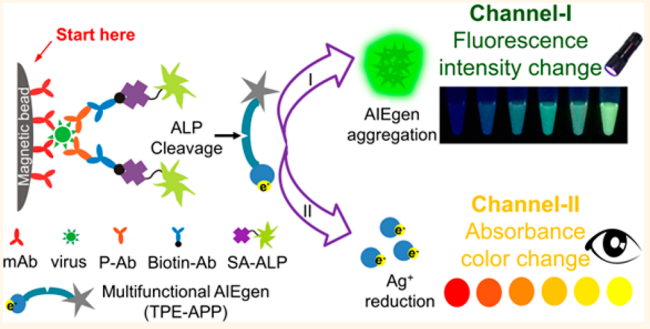

KEYWORDS: *fluorescence, naked-eye, dual-modality, immunoassay, aggregation-induced emission (AIE)*

An emerging and re-emerging spectrum of viral infectious pathogens, ranging from "A"vian influenza virus to "Z"ika virus with high incidence and mortality rates, severely threatens human health and has become one of the major public health concerns.[1] According to an official report by the World Health Organization (WHO) from January to February of 2017,[2] there were a total of 304 cases of human infection with H7N9 AIV (including 36 deaths). Another human enterovirus 71 (EV71) virus, which could cause severe hand, foot, and mouth disease (HFMD) in infants and young children, is currently one of the most contagious neurovirulent enterovirus in the third world countries.[3,4] The outbreaks of Zika virus (ZIKV) occurred quickly and spread out geographically with at least 84 countries/regions affected since 2007.[1] Therefore, it is critical to develop sensitive and accurate methods for virus clinical diagnosis, especially for the

Received: July 12, 2018
Accepted: August 27, 2018
Published: August 27, 2018

DOI: 10.1021/acsnano.8b05270
ACS Nano 2018, 12, 9549–9557

early stage of infection, to prevent virus spread and disease outbreaks. The traditional enzyme-linked immunosorbent assay (ELISA) based on the specific antigen−antibody reaction and enzymatic catalysis usually suffers from poor sensitivity.[5] Although PCR analysis features high sensitivity, the demands of intensive sample pretreatment and expensive instruments limit their wide applications in the point-of-care area.[6] More methods for virus detection, such as carbon nanotube array based assay,[7] microfluidic and microfluidic paper based analytical devices,[8−11] electrochemical sensors,[12,13] and flow cytometric methods,[14,15] have been developed in recent year.

Recently, colorimetric analytical strategies based on localized surface plasmon resonance (LSPR) properties of noble nanoparticle have been applied for various bioanalytes assay that could be discerned by naked-eye without the need of expensive instruments and complicated procedures.[16−23] These assays based on absorbance of the analytes, however, almost fade in accurate disease diagnosis for their poor sensitivity. With the rapid development of inorganic quantum dots (QDs) and organic fluorophores, fluorescence has been widely utilized in bioanalyte sensing with more than 1000 times enhancement in sensitivity compared to the plasmonic colorimetric assay.[24−38] Whereas the detection signals from these conventional fluorescent materials are compromised by their high background fluorescence and tend to decrease at high target concentration due to aggregation-caused quenching (ACQ) effect.[39,40] Unlike conventional organic fluorophores, AIEgens with propeller-shaped structures generally exhibit no or little emission in solution but enhanced emission in aggregated state, providing a superior choice for turn-on fluorescence candidate. The AIEgen aggregates exhibit advantages in luminosity, photobleaching resistance and biocompatibility. Although AIEgens have been widely used in analysis of enzymes, nucleic acids, cancer cells,[41−45] the application of AIE fluorescence as output signal for virus detection has not been demonstrated.

Herein, based on a multifuncational AIEgen, an ultrasensitive virion immunoassay platform with fluorescence and plasmonic colorimetry composed dual-modality read-out is presented (Scheme 1). We designed a water-soluble multifunctional AIEgen, named TPE-APP, with enzymatic cleavage sites (Figure S1). The single crystal structure (CDCC No. 1827833) confirmed its molecular structure (Figure 1). To couple the multifunctional AIEgen into the immunoassay system, the target virions were first captured by the immunomagnetic beads (IMNs), followed with the binding of rabbit polyclonal antibodies (P-Abs), biotinylated Abs (B-Abs), and the signal tags streptavidin-ALP (SA-ALP). The ALP enzyme could catalyze the hydrolysis of TPE-APP by removing its phosphoryl groups. The produced TPE-DMA was insoluble in water and could aggregate to emit out strong fluorescence with 380 times enhancement in intensity (Figure S2). This turn-on fluorescence signal was assigned as "Channel I" for accurate virus detection with its ultrahigh sensitivity. On the other hand, the hydrolysis of TPE-APP could simultaneously reduce Ag^+ to form a silver nanoshell around gold nanoparticles (AuNP). This shelling resulted in a pronounced plasmonic color change in a broad detection range that enable the convenient naked-eye based preliminary-screening of virus (Channel II in Scheme 1and Figure 1).

Scheme 1. Schematic Illustration of Fluorescent and Plasmonic Colorimetric Dual-Modality for Virus Detection Based on a Multifunctional AIEgen[a]

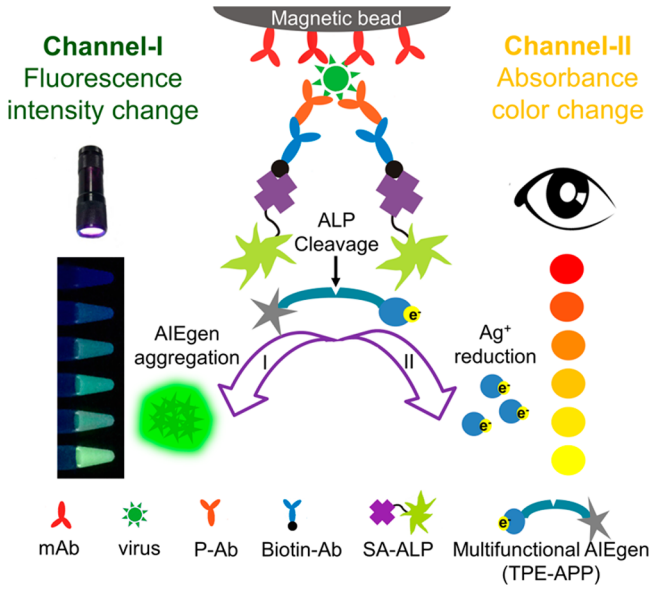

[a]P-Ab, polyclonal antibody; Biotin-Ab, biotinylated antibody; SA-ALP, alkaline phosphatase streptavidin.

RESULTS AND DISCUSSION

Establish Correlation Between the ALP Concentration and the Fluorescent and Plasmonic Colorimetric Signals. For its water-solubility, TPE-APP molecule did not emit out fluorescence in the DEA buffer. While in the presence of ALP, strong greenish blue fluorescence emitted out, indicating the efficient production of insoluble TPE-DMA aggregates (Figure 2a). To get the linear detection range, the TPE-APP concentration was first optimized to be 100 μM (Figure S3). When TPE-APP (100 μM) was incubated with different concentrations of ALP (0, 0.7, 1.4, 3.5 nM), the fluorescence intensity presented a gradual increase with the lasting of incubation time and saturated near 30 min (Figure 2b). The positive correlation between ALP concentration and the fluorescence intensity of AIE aggregates was also demonstrated by gradual increase of ALP concentration (Figure 2c). The specificity of the ALP enzyme to the multifunctional TPE-APP molecules was also confirmed by introducing other enzymes (Figure S4). Moreover, the phosphatase inhibitor Na_3VO_4 proved that the hydrolysis of TPE-APP was the result of ALP enzyme catalysis rather than the action of other substances in the solution (Figure S5). We then investigated the correlation between ALP hydrolysis and the colorimetric change. After incubation with ALP, characteristic absorption profile of AgNPs with a peak at 410 nm that different to the LSPR peak of 520 nm of AuNP could be observed. The intensity increased with the increase of ALP concentration (Figure 2d). And the color of the mixture quickly blue-shifted from red to yellow then to brown (Figure 2m). In contrast, the color of the mixture remained red in the absence of ALP (Table S1), indicating the indispensable role of ALP catalyzed hydrolysis in the reduction of Ag^+ and shelling of AuNP. The silver shelling on the surface of AuNP was further validated by TEM and high-resolution TEM images (Figure 2e−g). Energy dispersive X-ray spectroscopy (EDX) analyses also indicated that the nanoparticles were

DOI: 10.1021/acsnano.8b05270
ACS Nano 2018, 12, 9549−9557

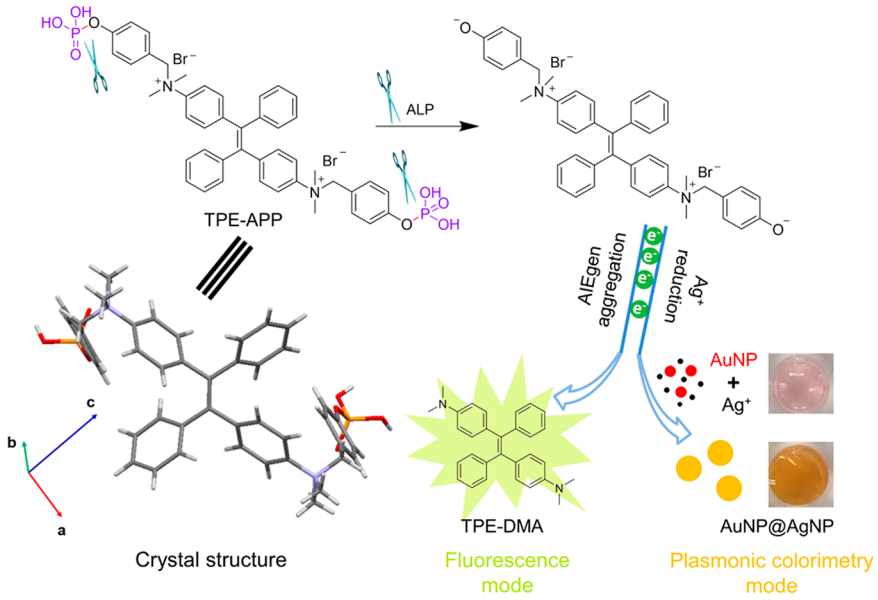

Figure 1. Reaction route and single crystal stucture of the multifunctional TPE-APP (CCDC ref number 1827833). We designed a water-soluble multifunctional AIEgen, named TPE-APP with an enzymatic cleavage site. It can be hydrolyzed by alkaline phosphatase (ALP) to remove the phosphoryl group, forming water insoluble TPE-DMA aggregates and a highly reactive species. The resulting TPE-DMA aggregate acts as a fluorescence signal because of its typical AIE properties. And the redox species could reduce silver ion to generate a silver nanoshell on the surface of AuNP (AuNP@AgNP). This leads to the blue shift of the LSPR peak of AuNPs, displaying a pronounced color change from red to yellow and further to brown. Such obvious plasmonic colorimetric change can be differentiated by the naked eye.

composed of Au and Ag elements. To confirm the distribution of each element in the AuNP@AgNP core−shell nanostructure, the high-angle annular dark field (HAADF)-STEM analysis was conducted. STEM-HAADF image revealed the typical AuNP@AgNP core−shell nanostructures with different atom numbers (Figure 2i), which were used as elemental mapping analysis. EDX elemental mapping analysis further showed that the Ag element was present at the surface (Figure 2j,k), indicating that Ag element had been localized on the surface of AuNP. Moreover, line-scanning profiling analysis showed that the Ag elements were homogeneously distributed surrounding the AuNP (Figure 2l). In sum, the catalyzed hydrolysis of TPE-APP constructed a dual-modality assay composed by a turn-on fluorescence and a naked-eye discernible colorimetric signal.

Efficient Capture of Target Virus. For proof of concept, the EV71 virus was detected by the dual-modility immunoassay after integrating with the high-efficiency immunomagnetic amplification. The conjugation of magnetic beads (MNs) with anti-VP1 mAb was demonstrated by immunofluorescence assay (Figure S6). The immunofluorescence results demonstrated the anti-VP1 mAbs have been successfully conjugated to the surface of MNs to form the IMNs for EV71 virus capture. The corresponding immuno-aggregation phenomenon was also confirmed by the scanning electron microscopy (SEM) images (Figure S7). In addition, the TEM image of intact EV71 virions with spherical structure is shown in Figure 3a. TaqMan real-time PCR (RT-qPCR) assays for the EV71 virions were carried out to test the efficiency of IMNs in capture of the target virus. The RT-qPCR curves showed that the different cycle threshold (C_t) values from different EV71 virion concentrations were responding to C_t value of the positive EV71 reference (Curve VI) (Figure 3b). Whereas no obvious peaks could be observed from IMNs alone or viruses incubated with nude MNs. Further analysis by agarose gel electrophoresis shows the reaction of the virus mixed with the IMNs all had corresponding gene fragments (lanes 2−5), consistent with the EV71 positive reference gene (lane 1). Whereas no fragments were observed when the EV71 virions were incubated with the nude MNs (lane 7), indicating the indispensable role of IMNs in capture of the target EV71 virions with high reliability and specificity (Figure S8). Besides, IMNs preserved their colloidal stability and virus capture ability during 6 days of storage (Figure S9). The use of IMNs as immunoreaction platform in our strategy could simplify the sample preparation process, improve the enrichment efficiency, and amplify the detection signal due to their fast magnetic responsiveness and slow loss rate.[16,17,29,30,46] Meanwhile, abundant binding sites expressed on the surface of virions[4] can further amplify the detection signal of the immunoassay.

Specific and Sensitive Dual-Modality Immunoassay. The specificity and anti-interference capability of this immunoassay for EV71 virion detection were next evaluated. P-Abs, B-Abs, and SA-ALP were used as immune signal amplification tags to react with EV71 virions-IMNs to form sandwich-structure immunocomplexes. One reagent blank and five other enteroviruses as negative samples including CVA2, CVA4, CVA6, CVA16, and ECHO-18 were tested using our proposed method. Strong fluorescence was readily emitted out in the EV71 virus sample, while no obvious fluorescence was found in the negative sample (Figure 3c). Because the negative samples could not bridge the conjugation immunocomplex and after washing off, there was no ALP to hydrolyze the TPE-APP to form the fluorescent TPE-DMA aggregates. It revealed that the fluorescence assay possessed a good specificity toward virus detection. The specificity of the immunoassay for virus can also be detected by naked eye in the colorimetric modality. Only in the presence of target EV71 virions, could yellow color be observed (Figure 3d). These results demonstrated that the

DOI: 10.1021/acsnano.8b05270
ACS Nano 2018, 12, 9549−9557

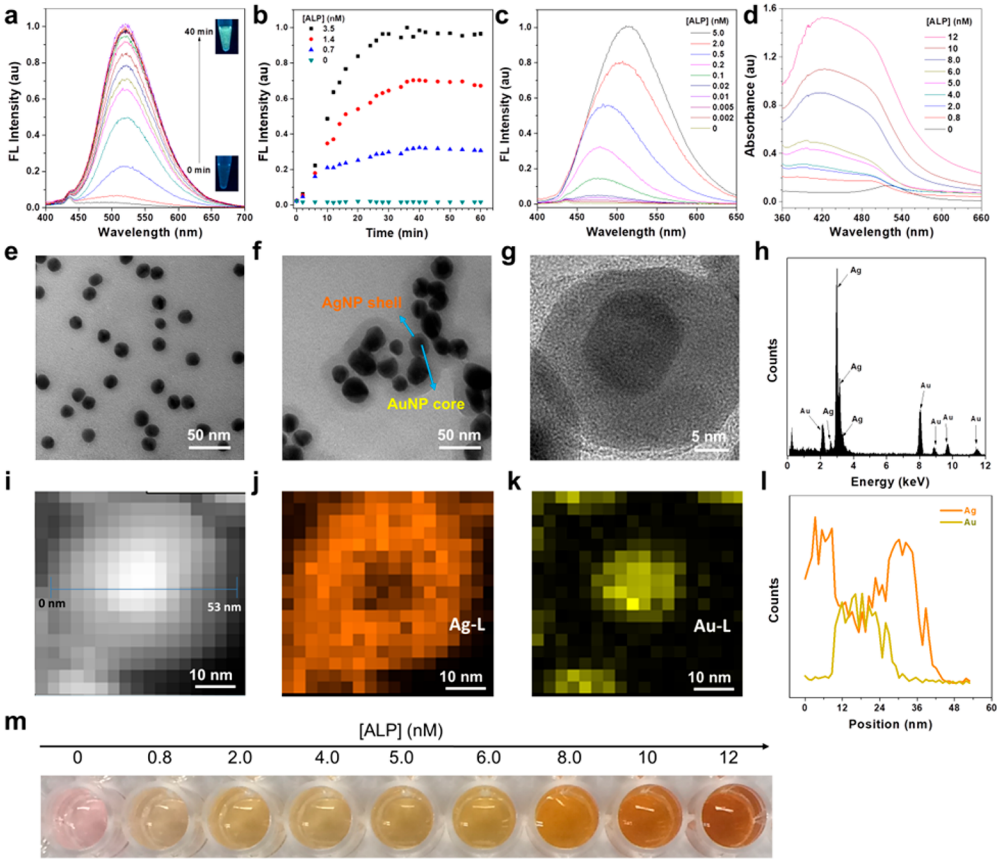

Figure 2. Establishment of fluorescence and plasmonic colorimetry based dual-modality detection method. (a) Fluorescence spectra evolution of the mixture of TPE-APP (100 μM) and ALP (3.5 nM) during 40 min incubation time. (b) Plotting of fluorescence intensity *versus* incubation time in the presence of various concentrations of ALP. (c) Fluorescence spectra of the mixture of TPE-APP (100 μM) and various concentrations of ALP after 30 min incubation. (d) Absorption spectra of the mixture of AuNP (3.2 nM), Ag^+ (1.2 mM), and TPE-APP (100 μM) with various concentrations of ALP after 30 min incubation. (e) TEM image of AuNP. (f) TEM image of AuNP@AgNP produced by ALP (6 nM). (g) HRTEM image and (h) EDX profile of AuNP@AgNP. (i) STEM-HAADF image, (j) Ag element, and (k) Au element mapping of AuNP@AgNP, respectively. (l) EDXS line profile for image (h). (m) Photograph of the color change in (d).

dual-modality immunoassay was of high specificity in EV71 detection.

To evaluate the sensitivity and linear analytic range of our dual-modality immunoassay, various concentrations of EV71 virions were tested. As shown in Figure S10, the detection solution gradually changed from red to dark brown with the EV71 virus concentration increasing. This colorimetric change was a result of the different amount of Ag atom shelling on the AuNP surface. The color change of detection solution was verified *via* the blue shifting of the absorption spectra (Figure 4a). The absorption peaks at around 410 nm for detection solutions with different colors were intensified with increasing amount of EV71 virions. An excellent linear relationship yielded from 1.34×10^6 to 1.34×10^8 copies/mL with a linear correlation coefficient (R^2) of 0.996 by plotting the absorbance at 410 nm with EV71 virion concentrations. The limit of detection (LOD) was calculated to be 868.4 copies/μL (Figure 4b). The limit of detection is defined as virus concentration at which the absorbance measured at 410 nm (A_{410}) is equivalent to the average A_{410} of the blank control plus three times its standard deviation. As we know, the fluorescence assay is more sensitive than the absorption assay, and we could use the fluorescence modality for ultrasensitive detection and accurate diagnosis. As expected, the fluorescence signal could be detected even in the presence of ultralow concentration of virus (Figure 4c). A good linear relationship was obtained in the viral concentration range of 1.67×10^3–2.505×10^5 copies/mL with R^2 of 0.992 (Figure 4d). The limit of detection was determined to be 1.4 copies/μL, nearly 1000-fold enhancement comparing to that in the absorption modality. The sensitivity of the dual-modality immunoassay for virus detection is competitive with those of other sensitive analytical methods including fluorescent/absorption and electroluminescent measurements (Table S2).[7,8,12,13,17,20,29,46–48] These results suggested that our dual-modality immunoassay possessed advantages including high sensitivity, good quantitative capability and wide linear detection range that could be applied for not only convenient preliminary-screening, but also accurate diagnosis of virus infection.

Dual-Modality Immunoassay for EV71 Virus Detection in Clinical Sample. Encouraged by the high sensitivity and good specificity of the multifunctional AIEgens based dual-modality assay, real clinical samples were tested. Twenty-four throat and cloacal swab samples from HFMD patients were randomly collected. We employed our immunoassay to detect these clinical samples. As a result, 8 out of 24 samples were detected to be positive *via* plasmonic colorimetry (Figure 5), confirming by the absorbance at 410 nm above the threshold value. Contributed by the pretty higher sensitivity of the fluorescence signal, another 2 samples were detected to be

DOI: 10.1021/acsnano.8b05270
ACS Nano 2018, 12, 9549–9557

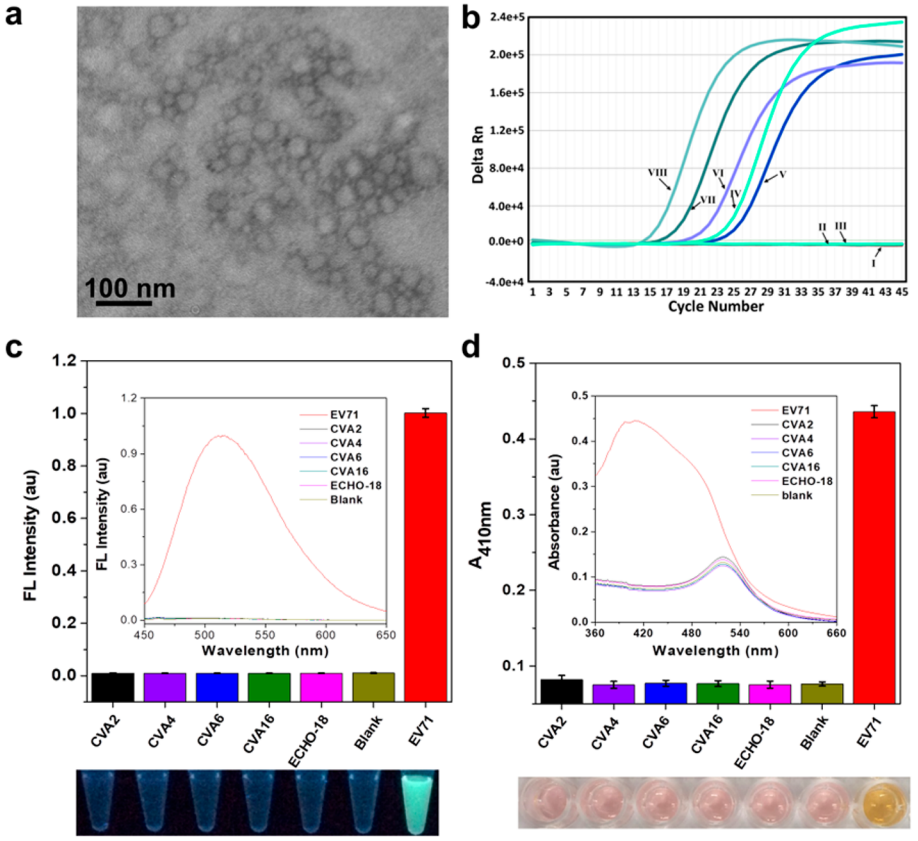

Figure 3. Specificity test of the dual-modality immunoassay for EV71 virion detection. (a) TEM image of purified EV71 virions. (b) RT-qPCR analysis for the captured EV71 virions using IMNs. Curves V−VIII correspond to the EV71 concentrations of 5×10^8, 5×10^9, 5×10^{10}, and 5×10^{11} copies/mL, respectively, whereas the C_t value were 22.69, 19.04, 16.11, and 14.33, respectively. Curves I and II were MNs and IMNs, respectively; curves III and IV were EV71 virion negative reference and positive reference (C_t value of 21.36), respectively. (c) Fluorescence intensity of various kinds of viruses, with fluorescence spectra and a photograph under 365 nm UV lamp in the inset and underneath, respectively. (d) Absorbance at 410 nm of various kinds of viruses, with absorption spectra and photograph under ambient light in the inset and underneath, respectively.

positive which presented 100% clinical accuracy referring to the standard RT-qPCR results (Figures 5 and S11; Table S3). These results strongly demonstrate that our dual-modality based immunoassay possessed a strong anti-interference ability, high accuracy as well as high sensitivity.

Comparing with traditional single modality assay, our dual-modality immunoassay based on the multifunctional AIEgens displayed the following advantages. First, our approach integrates fluorescent and plasmonic colorimetric modalities into one detection system, from which the analysis results not only can be preliminarily screened based on the obvious colorimetric change *via* naked-eye observation, but also can be accurately diagnosed by fluorescence signal with significantly enhanced sensitivity. Second, such a "turn-on" featured AIE biosensor possesses nearly no background signal and could offer advantages in accuracy, reliability, and strong anti-interference capability. Traditional organic fluorophore or QD based assays are easily experiencing emission quenching when confronting a complex environment, resulting in compromised sensitivity and poor signal-to-noise ratio. Third, such dual-modality immunoassay based on multifunctional AIEgen does not require complicated sample pretreatment or sophisticated instruments, which makes it suitable for both domestic and hospital requirements. Finally, our detection strategy is universal and can be straightforwardly extended to the specific detection of other types of virus, such as H7N9 and Zika virus, just through changing the conjugated antibody (Figures S12 and S13).

CONCLUSIONS

In summary, we designed a convenient dual-modality readout immunoassay platform based on a multifunctional AIEgen for highly sensitive and specific detection of virus by integrating of fluorescence and plasmonic colorimetry in a single detection system. The multifunctional AIEgen with enzyme cleavage sites could be hydrolyzed by virus immunobridged ALP, with production of strong emissive AIE aggregates. And at the same time, Ag^+ could be reduced to an *in situ* shell on the surface of AuNP with an obvious color change for naked-eye observation. Further by taking advantage of the magnetic enrichment, EV71 virions can be specifically assayed with a detection limit down to 1.4 copies/μL. Even more importantly, this dual-modality immunoassay can be applied for real clinical sample diagnosis. Other pathogens, such as H7N9 virus and Zika virus, can also be detected by simple changing the conjugated antibodies. The multifunctional AIE molecule, dual-signal readout, excellent quantitatively capability, high sensitivity and strong anti-interference ability collectively construct a promising platform for both convenient preliminary screening and high-accuracy clinic diagnosis of virus.

DOI: 10.1021/acsnano.8b05270
ACS Nano 2018, 12, 9549−9557

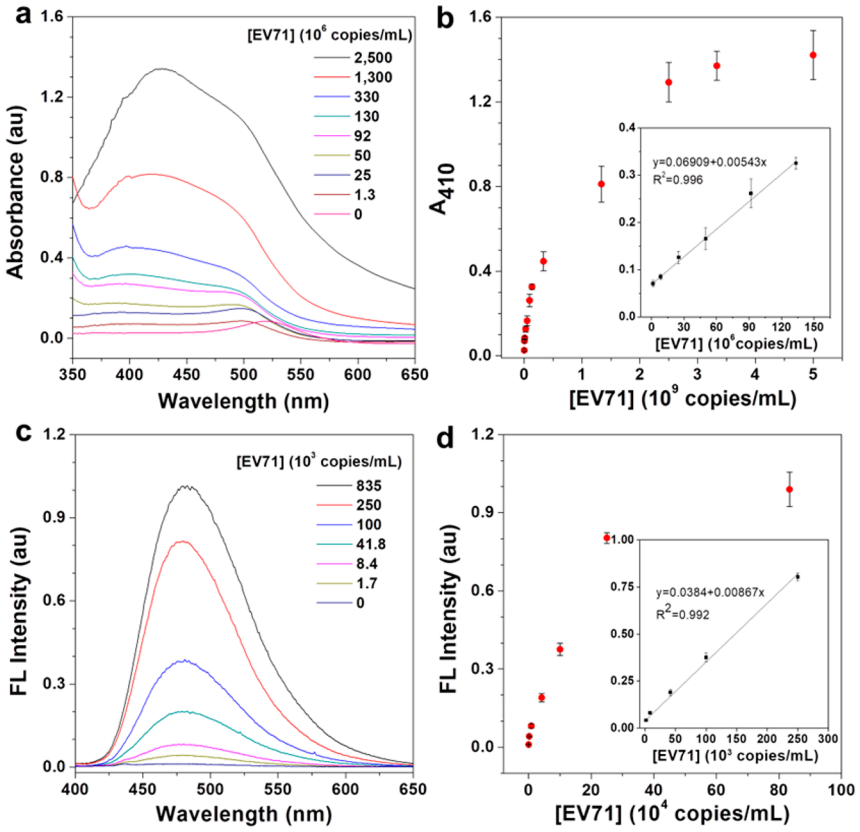

Figure 4. Sensititity test of the dual-modality inmmunoassay for EV71 virion detection. (a) Absorption spectra with various concentrations of EV71. (b) Plotting of absorbance at 410 nm *versus* EV71 concentrations, with the linear detection range in the inset. (c) Fluorescence spectra with ultralow concentrations of EV71. (d) Plotting of fluorescence intensity *versus* the EV71 concentration, with the linear detection range in the inset.

METHODS

Synthesis of AuNPs. The citrate-capped AuNPs with the diameter of about 13 nm were prepared by sodium citrate reduction of $HAuCl_4$.[25] Before this experiment, all glassware was cleaned with freshly prepared aqua regia (HCl/HNO_3, 3:1) and then rinsed with doubly distilled water. A volume of 30 mL of 0.01% $HAuCl_4$ was heated to boiling with vigorous stirring, and 1 mL of 1% trisodium citrate was added under stirring. After appearance of a burgundy color, boiling and stirring were continued for 30 min. The solution was stirred until the colloid reached room temperature. The solution was stored at 4 °C for further use.

Optimization of TPE-APP Concentration and Incubation Time for ALP Activity Assay. To optimize TPE-APP concentration, TPE-APP at a series of the final concentrations (0−500 μM) in diethanolamine buffer (DEA; 10 mM, pH 9.8, containing 0.1 mM $MgCl_2$) were hydrolyzed by ALP (1.05 nM), the mixture was incubated for 30 min at 37 °C. The fluorescence spectra of the hydrolyzed production were recorded using a Horiba FluoroLog-3 fluorescence spectrophotometer. For the kinetic study, different amounts of ALP were added into the TPE-APP solution (100 μL, 100 μM), and then incubated at 37 °C for 40 min. The enzymatic hydrolysis process was monitored by the fluorescence spectra measurements.

Colorimetric Detection of ALP Activity *via* the Controlled Growth of AgNPs on the Surface of AuNPs. The enzymatic reaction was carried out in a 96-well plate by incubating mixtures of different amounts of ALP and TPE-APP in DEA buffer (pH 9.8, 10 mM, containing 0.1 mM $MgCl_2$) at 37 °C for 30 min. The final concentration of TPE-APP in the 96-well plate was fixed to be 100 μM, and the ALP concentration ranged from 0 to 12 nM. Then AuNPs (final concentration: 3.2 nM) and $AgNO_3$ (final concentration: 1.2 mM) solution were added into the enzymatic reaction mixture in the 96-well plate. The AuNPs solution would undergo a quick color change within 30 min at room temperature. The UV−vis absorption spectra and the absorbance at 410 nm of the resulting AuNP@AgNP solution were taken on a PerkinElmer Lambda 25 UV−vis absorption spectrophotometer. The transmission electron microscopy (TEM) images were obtained by using a HITACHI H-7650 electron microscope with an acceleration voltage of 80 kV. HRTEM observation and the linear EDX elemental distribution were carried out with Tecnai G2 F30 (FEI, Holland) for composition analysis. The samples of AuNPs and AuNP@AgNPs for TEM were prepared by dropping 7 μL of each sample onto ultrathin carbon film copper grids.

Preparation of Immunomagnetic Beads with mAb-VP1. According to the protocol as in our previous report, EDC and NHS were used to activate the carboxyl groups on the superparamagnetic beads (MNs) with the size of 500 nm.[17,29] Briefly, incubating 10 μL of the MNs (50 mg/mL) with 50 mM EDC and 50 mM NHS in 400 μL of MES buffer (0.1 M MES, 0.15 M NaCl, pH 6.5) for 30 min at 37 °C, the MNs were separated and washed with 1× PBS buffer (pH 7.4) three times. Then the activated MNs were covalently coupled with 20 μL of 0.5 mg/mL anti-VP1 mAbs for 4 h at 37 °C to form the immunomagnetic beads (mAb-VP1 bound MNs, IMNs). The IMNs with the concentration of 1 mg/mL were kept in 500 μL of 1× PBS (pH 7.4) containing 1% (w/v) BSA and 0.05% (w/v) NaN_3 at 4 °C for further use. The characterization of IMNs is described in detail in Figures S6 and S7. Furthermore, using other monoclonal antibodies attached to the MNs, mAb-HA bound MNs and mAb-Zika bound MNs were successfully prepared according to the same method mentioned above.

Turn on AIEgens Derived Fluorescence and Naked-Eye Dual-Modality Immunoassay for Virion Detection. Taking the EV71 virion detection, for example, the TEM image of EV71 virions was obtained with a HITACHI H-7650 electron microscope (Figure

DOI: 10.1021/acsnano.8b05270
ACS Nano 2018, 12, 9549−9557

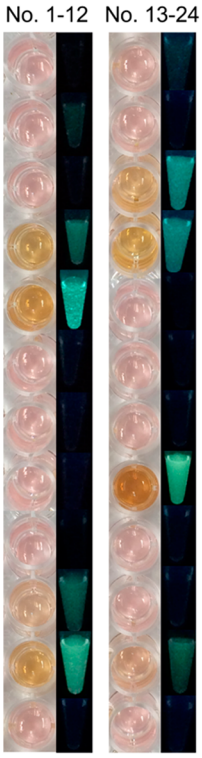

Sample No.	Dual-modality			RT-qPCR
	Abs	FL	Result	
1	0.073	0.006	×	×
2	0.063	0.043	√	√
3	0.070	0.006	×	×
4	0.334	0.248	√	√
5	0.482	0.513	√	√
6	0.061	0.005	×	×
7	0.065	0.004	×	×
8	0.070	0.006	×	×
9	0.061	0.006	×	×
10	0.126	0.163	√	√
11	0.336	0.509	√	√
12	0.071	0.005	×	×
13	0.064	0.024	√	√
14	0.075	0.005	×	×
15	0.248	0.387	√	√
16	0.417	0.244	√	√
17	0.071	0.005	×	×
18	0.053	0.004	×	×
19	0.065	0.004	×	×
20	0.669	1.000	√	√
21	0.061	0.003	×	×
22	0.060	0.004	×	×
23	0.123	0.131	√	√
24	0.065	0.004	×	×

Figure 5. Practicability test of the dual-modality inmmunoassay for real clinical samples detection. Twenty-four clinical samples from enterovirus-infectious HFMD patients were randomly arranged and detected by using our dual-modality immunoassay with standard RT-qPCR analysis confirmation. Green color number means lower than threshold and is detected to be negative without virus infetion risk. Red color number means higher than threshold and is detected to be positive with virus infection risk. The detection result is diagnosed to be positive if any one modilitity shows positive result. √ means positive result and × means negative result.

3a). And the virus was quantitated by using TaqMan real-time RT-PCR to determine the exact copy number of virus sample.[46] The whole procedure of dual-modality immunoassay is outlined in Scheme 1. An amount of 50 μL of 1 mg/mL IMNs was washed twice with wash buffer (PBST, consisting of 0.1% Tween 20 in 1× PBS buffer (pH 7.4)). Then different amounts of EV71 virions were added to the IMNs in a 2 mg/mL solution of BSA-PBS with a final volume of 100 μL (pH 7.4), and the mixture was incubated for 30 min at 37 °C with gentle shaking. Then the resulting bead-virus composites were separated and washed three times with 400 μL PBST. After the composites were incubated with rabbit polyclonal anti-VP1 Abs (5 μg/mL) in 200 μL of blocking buffer (BB, consisting 2 mg/mL BSA in 1× PBS buffer (pH 7.4)), for 1 h at 37 °C with gentle shaking. The composites were washed three times with PBST, and 10 μg/mL biotinylated goat anti-rabbit secondary Abs in 100 μL of BB was added for 1 h with gentle shaking. After washing three times with PBST, the diluted SA-ALP with 1:10 in BB was added to the composites above, and incubated for 30 min at 37 °C. The formed immunocomplexes were separated and washed with PBST for three times. Subsequently, 10 μL of TPE-APP (10 mM) in DEA buffer (pH 9.8, 10 mM, containing 0.1 mM $MgCl_2$) with a final volume of 100 μL was added to the formed sandwich-structure immunocomplexes above and then incubated for 30 min at 37 °C. Afterward, the suspension was separated from the IMBs with a magnetic scaffold and collected for fluorescence spectrum measurements by a Fluorolog-3 (Horiba Jobin Yvon) fluorescence spectrometer, and the EV71 virion could be detected by the fluorescence assay. Or the suspension was separated and added to a new 96-well plate which contained 1.2 μL of 100 mM $AgNO_3$ and 1 μL of 320 nM AuNPs. The AuNPs solution would undergo a quick color change within 30 min, and the EV71 virions could be detected by the naked eye. The UV−vis spectra and the absorbance at 410 nm were measured to quantify the virus concentration. The dual-modality immunoassay for EV71 virion detection has been constructed based on the mentioned above. For the specificity of the immunoassay, six control experiments were also performed: the five control experiments with several other common enteroviruses (CVA2, CVA4, CVA6, CVA16, and ECHO-18) were used as negative samples, and another control experiment using 2% BSA-PBS without any virus as reagent blank was also performed the same procedure as the EV71 sample.

Taqman Real-Time PCR Assay. The viral RNA of different concentrations of EV71 captured by IMNs was extracted using the High Pure Viral RNA Kit (Roche) according to the manufacturer's protocols. TaqMan real-time PCR was performed following the manufacturer's instructions of EV71 RNA TaqMan Real-Time Detection Kit (Bioperfectus Technologies). The 25 μL of reaction volume consisted of 7.5 μL of RT-PCR reaction solution, 5 μL of enzyme reaction solution, 4 μL of EV71 reaction solution, 3.5 μL of free RNase water, and 5 μL of RNA sample. The reaction was run on a 7500 Real-Time PCR System (Applied Biosystems). The PCR conditions were as follows: 1 cycle of 50 °C for 30 min, 1 cycle of 95 °C for 5 min, 45 cycles of 95 °C for 10 s, and 45 cycles of 55 °C for 40 s, with real-time detection at the end of 45 cycles of 55 °C for 40 s.

Dual-Modality Immunoassay for EV71 Virus Detection in Clinical Sample. The clinical samples containing human throat and cloacal swab samples from 24 different enterovirus-infectious HFMD patients were collected and treated with Hank's balanced salt solution (1× HBSS), including 10 EV71-infectious HFMD patients and 14 other enterovirus-infectious HFMD patients. These treated samples were then detected using the same protocol described above. Furthermore, TaqMan real-time PCR for EV71 virion detection was also performed to validate our proposed method for practical applications with highly stable and sensitive.

ASSOCIATED CONTENT

Supporting Information

The Supporting Information is available free of charge on the ACS Publications website at DOI: 10.1021/acsnano.8b05270.

Experimental details, AIE property of TPE-DMA; optimization of TPE-APP concentration; fluorescence spectra; characterization of immunomagnetic beads; RT-qPCR analysis; specificity of dual-modality immunoassay; ^{1}H NMR, ^{31}P spectra, and ^{13}C NMR spectra (PDF)

Crystal data for TPE-APP (CIF)

AUTHOR INFORMATION

Corresponding Authors

*E-mail: cjinquan@szcdc.net.
*Email: renlizhang@szcdc.net.
*E-mail: tangbenz@ust.hk.

ORCID

Xuewen He: 0000-0002-8414-5164
Ryan T. K. Kwok: 0000-0002-6866-3877
Renli Zhang: 0000-0003-0983-6528
Ben Zhong Tang: 0000-0002-0293-964X

Author Contributions

L.H.X., X.H., and Z.Z. contributed equally to the work. L.H.X. and X.H. conceived the original idea for this study. L.H.X. and X.H. designed the experiments. X.H., L.H.X., and Z.Z. designed the molecules. X.H synthesized the molecules with help from Z.Z; Y. X and H. H. Y. S. obtained the single crystal structure. L.H.X. did all the other experiments including virus

DOI: 10.1021/acsnano.8b05270
ACS Nano 2018, 12, 9549−9557

proliferation, extraction, detection, characterization, and calculation. B.Z.T. supervised the whole process. B.Z.T., L.H.X., X.H., and R.T.K.K. discussed for the manuscript. L.H.X. wrote the manuscript, and X.H., Z.Z., and R.T.K.K. revised the manuscript. All the authors participated in data analysis.

Notes

The authors declare no competing financial interest.

ACKNOWLEDGMENTS

The authors acknowledge funding to B.Z.T. from the Innovation and Technology Commission (ITC-CNERC14SC01 and ITS/254117), The National Science Foundation of China (21788102), the Research Grants Council of Hong Kong (16301614, 16305015, N_HKUST604/14, A-HKUST605/16, and C6009-17G), and the Science and Technology Plan of Shenzhen (JCYJ20160229205601482). L.H.X is grateful for the support from the National Natural Science Foundation of China (21705111), the Shenzhen Science and Technology Innovation Project (JCYJ20160428142912690), and Shenzhen Health and Family Planning Commission Project (SZBC2017004, SZSM201611064).

REFERENCES

(1) Gao, F. From "A"IV to "Z"IKA: Attacks from Emerging and Re-emerging Pathogens. *Cell* **2018**, *172*, 1157−1159.

(2) W.H.O. website. Human Infection with Avian Influenza A (H7N9) Virus. Update 20 February 2017, http://www.who.int/csr/don/20-february-2017-ah7n9-china/en/.

(3) Wang, T.; Wang, B.; Huang, H.; Zhang, C.; Zhu, Y.; Pei, B.; Cheng, C.; Sun, L.; Wang, J.; Jin, Q.; Zhao, Z. Enterovirus 71 Protease 2Apro and 3Cpro Differentially Inhibit the Cellular Endoplasmic Reticulum-Associated Degradation (ERAD) Pathway *via* Distinct Mechanisms, and Enterovirus 71 Hijacks ERAD Component p97 to Promote Its Replication. *PLoS Pathog.* **2017**, *13*, e1006674.

(4) Wang, X.; Peng, W.; Ren, J.; Hu, Z.; Xu, J.; Lou, Z.; Li, X.; Yin, W.; Shen, X.; Porta, C.; Walter, T.; Evans, G.; Axford, D.; Owen, R.; Rowlands, D.; Wang, J.; Stuart, D.; Fry, E.; Rao, Z. A Sensor Adaptor Mechanism for Enterovirus Uncoating from Structures of EV71. *Nat. Struct. Mol. Biol.* **2012**, *19*, 424−429.

(5) Yolken, R. H. Enzyme-Linked Immunosorbent-Assay (ELISA): A Practical Tool for Rapid Diagnosis of Viruses and Other Infectious Agents. *Yale J. Biol. Med.* **1980**, *53*, 85−92.

(6) Lee, M.; Chang, P.; Shien, J.; Cheng, M.; Shieh, H. Identification and Subtyping of Avian Influenza Viruses by Reverse Transcription PCR. *J. Virol. Methods* **2001**, *97*, 13−22.

(7) Yeh, Y.; Tang, Y.; Sebastian, A.; Dasgupta, A.; Perea-Lopez, N.; Albert, I.; Lu, H.; Terrones, M.; Zheng, S. Tunable and Label-Free Virus Enrichment for Ultrasensitive Virus Detection Using Carbon Nanotube Arrays. *Sci. Adv.* **2016**, *2*, e1601026.

(8) Yu, X.; Xia, Y.; Tang, Y.; Zhang, W.-L.; Yeh, Y.; Lu, H.; Zheng, S. A Nanostructured Microfluidic Immunoassay Platform for Highly Sensitive Infectious Pathogen Detection. *Small* **2017**, *13*, 1700425.

(9) Xia, Y.; Tang, Y.; Yu, X.; Wan, Y.; Chen, Y.; Lu, H.; Zheng, S. Label-Free Virus Capture and Release by a Microfluidic Device Integrated with Porous Silicon Nanowire Forest. *Small* **2017**, *13*, 1603135.

(10) Hong, S.-L.; Zhang, Y.-N.; Liu, Y.-H.; Tang, M.; Pang, D.-W.; Wong, G.; Chen, J.; Qiu, X.; Gao, G.; Liu, W.; Bi, Y.; Zhang, Z.-L. Cellular-Beacon-Mediated Counting for the Ultrasensitive Detection of Ebola Virus on an Integrated Micromagnetic Platform. *Anal. Chem.* **2018**, *90*, 7310−7317.

(11) Mu, X.; Zhang, L.; Chang, S.; Cui, W.; Zheng, Z. Multiplex Microfluidic Paper-Based Immunoassay for the Diagnosis of Hepatitis C Virus Infection. *Anal. Chem.* **2014**, *86*, 5338−5344.

(12) Wu, Z.; Hu, J.; Zeng, T.; Zhang, Z.; Chen, J.; Wong, G.; Qiu, X.; Liu, W.; Gao, G.; Bi, Y.; Pang, D.-W. Ultrasensitive Ebola Virus Detection Based on Electroluminescent Nanospheres and Immunomagnetic Separation. *Anal. Chem.* **2017**, *89*, 2039−2048.

(13) Sun, A. A Potentiometric Immunosensor for Enterovirus 71 based on Bis-MPA-COOH Dendrimer-Doped AgCl Nanospheres with a Silver Ion-Selective Electrode. *Analyst* **2018**, *143*, 487−492.

(14) Brussaard, C. P. D.; Marie, D.; Bratbak, G. Flow Cytometric Detection of Viruses. *J. Virol. Methods* **2000**, *85*, 175−182.

(15) Martín, J.; Lazo, L.; Valdés, I.; Gil, L.; Romero, Y.; Castro, J.; Guillén, G.; Hermida, L. Comparison of Two Methods with Potential Application in the Detection of Viremia Produced by Clinical Dengue Virus Isolates. *Bionatura* **2016**, *1*, 67−70.

(16) Zhou, C.; Zhao, J.; Pang, D.-W.; Zhang, Z.-L. Enzyme-Induced Metallization as a Signal Amplification Strategy for Highly Sensitive Colorimetric Detection of Avian Influenza Virus Particles. *Anal. Chem.* **2014**, *86*, 2752−2759.

(17) Xiong, L.-H.; He, X.; Xia, J.; Ma, H.; Yang, F.; Zhang, Q.; Huang, D.; Chen, L.; Wu, C.; Zhang, X.; Zhao, Z.; Wan, C.; Zhang, R.; Cheng, J. Highly Sensitive Naked-Eye Assay for Enterovirus 71 Detection Based on Catalytic Nanoparticle Aggregation and Immunomagnetic Amplification. *ACS Appl. Mater. Interfaces* **2017**, *9*, 14691−14699.

(18) Rodríguez-Lorenzo, L.; de la Rica, R.; Álvarez-Puebla, R. A.; Liz-Marzán, L. M.; Stevens, M. M. Plasmonic Nanosensors with Inverse Sensitivity by Means of Enzyme-Guided Crystal Growth. *Nat. Mater.* **2012**, *11*, 604−607.

(19) de la Rica, R.; Stevens, M. M. Plasmonic ELISA for the Ultrasensitive Detection of Disease Biomarkers with the Naked Eye. *Nat. Nanotechnol.* **2012**, *7*, 821−824.

(20) Liu, D.; Wang, Z.; Jin, A.; Huang, X.; Sun, X.; Wang, F.; Yan, Q.; Ge, S.; Xia, N.; Niu, G.; Liu, G.; Hight, W.; Chen, X. Acetylcholinesterase-Catalyzed Hydrolysis Allows Ultrasensitive Detection of Pathogens with the Naked Eye. *Angew. Chem., Int. Ed.* **2013**, *52*, 14065−14069.

(21) Qu, W.; Liu, Y.; Liu, D.; Wang, Z.; Jiang, X. Copper-Mediated Amplification Allows Readout of Immunoassays by the Naked Eye. *Angew. Chem., Int. Ed.* **2011**, *50*, 3442−3445.

(22) Wei, J.; Zheng, L.; Lv, X.; Bi, Y.; Chen, W.; Zhang, W.; Shi, Y.; Zhao, L.; Sun, X.; Wang, F.; Cheng, S.; Yan, J.; Liu, W.; Jiang, X.; Gao, G.; Li, X. Analysis of Influenza Virus Receptor Specificity Using Glycan-Functionalized Gold Nanoparticles. *ACS Nano* **2014**, *8*, 4600−4607.

(23) Chu, C.; Ge, S.; Zhang, J.; Lin, H.; Liu, G.; Chen, X. Enzyme-Free Colorimetric Determination of EV71 Virus Using a 3D-MnO_2-PEG Nanoflower and 4-MBA-MA-AgNPs. *Nanoscale* **2016**, *8*, 16168−16172.

(24) He, X.; Ma, N. Biomimetic Synthesis of Fluorogenic Quantum Dots for Ultrasensitive Label-Free Detection of Protease Activities. *Small* **2013**, *9*, 2527−2531.

(25) He, X.; Zeng, T.; Li, Z.; Wang, G.; Ma, N. Catalytic Molecular Imaging of MicroRNA in Living Cells by DNA-Programmed Nanoparticle Disassembly. *Angew. Chem., Int. Ed.* **2016**, *55*, 3073−3076.

(26) He, X.; Li, Z.; Chen, M.; Ma, N. DNA-Programmed Dynamic Assembly of Quantum Dots for Molecular Computation. *Angew. Chem., Int. Ed.* **2014**, *53*, 14447−14450.

(27) He, X.; Ma, N. A General Strategy for Label-free Sensitive DNA Detection Based on Quantum Dot Doping. *Anal. Chem.* **2014**, *86*, 3676−3681.

(28) Li, Z.; Wang, G.; Shen, Y.; Guo, N.; Ma, N. DNA-Templated Magnetic Nanoparticle-Quantum Dot Polymers for Ultrasensitive Capture and Detection of Circulating Tumor Cells. *Adv. Funct. Mater.* **2018**, *28*, 1707152.

(29) Xiong, L.-H.; Cui, R.; Zhang, Z.-L.; Yu, X.; Xie, Z.; Shi, Y.; Pang, D.-W. Uniform Fluorescent Nanobioprobes for Pathogen Detection. *ACS Nano* **2014**, *8*, 5116−5124.

(30) Wen, C.-Y.; Wu, L.; Zhang, Z.; Liu, Y.; Wei, S.; Hu, J.; Tang, M.; Sun, E.; Gong, Y.; Yu, J.; Pang, D.-W. Quick-Response Magnetic

DOI: 10.1021/acsnano.8b05270
ACS Nano 2018, 12, 9549−9557

Nanospheres for Rapid, Efficient Capture and Sensitive Detection of Circulating Tumor Cells. *ACS Nano* **2014**, *8*, 941−949.
(31) Ma, W.; Fu, P.; Sun, M.; Xu, L.; Kuang, H.; Xu, C. Dual Quantification of MicroRNAs and Telomerase in Living Cells. *J. Am. Chem. Soc.* **2017**, *139*, 11752−11759.
(32) Wu, X.; Hao, C.; Kumar, J.; Kuang, H.; Kotov, N. A.; Liz-Marzan, L. M.; Xu, C. Environmentally Responsive Plasmonic Nanoassemblies for Biosensing. *Chem. Soc. Rev.* **2018**, *47*, 4677−4696.
(33) Labib, M.; Mohamadi, R. M. M.; Poudineh, M.; Ahmed, S. U.; Ivanov, I.; Huang, C.; Moosavi, M.; Sargent, E. H.; Kelley, S. O. Single-Cell mRNA Cytometry *via* Sequence-Specific Nanoparticle Clustering and Trapping. *Nat. Chem.* **2018**, *10*, 489−495.
(34) Poudineh, M.; Aldridge, P.; Ahmed, S.; Green, B.; Kermanshah, L.; Nguyen, V.; Tu, C.; Mohamadi, R.; Nam, R.; Hansen, A.; Sridhar, S.; Finelli, A.; Fleshner, N.; Joshua, A.; Sargent, E. H.; Kelley, S. O. Tracking the Dynamics of Circulating Tumour Cell Phenotypes Using Nanoparticle-Mediated Magnetic Ranking. *Nat. Nanotechnol.* **2017**, *12*, 274−281.
(35) Kelley, S. O. Advancing Ultrasensitive Molecular and Cellular Analysis Methods to Speed and Simplify the Diagnosis of Disease. *Acc. Chem. Res.* **2017**, *50*, 503−507.
(36) Lin, S.; Yang, X.; Jia, S.; Weeks, A.; Hornsby, M.; Lee, P.; Nichiporuk, R.; Iavarone, A.; Wells, J.; Toste, F.; Chang, C. J. Redox-Based Reagents for Chemoselective Methionine Bioconjugation. *Science* **2017**, *355*, 597−602.
(37) Bai, H.; Lu, H.; Fu, X.; Zhang, E.; Lv, F.; Liu, L.; Wang, S. Supramolecular Strategy Based on Conjugated Polymers for Discrimination of Virus and Pathogens. *Biomacromolecules* **2018**, *19*, 2117−2122.
(38) Li, J.; Baird, M. A.; Davis, M. A.; Tai, W.; Zweifel, L. S. Z.; Waldorf, K. M. A.; Gale, M., Jr; Rajagopal, L.; Pierce, R. H.; Gao, X. Dramatic Enhancement of the Detection Limits of Bioassays *via* Ultrafast Deposition of Polydopamine. *Nat. Biomed. Eng.* **2017**, *1*, 0082.
(39) Luo, J.; Xie, Z.; Lam, J. W.; Cheng, L.; Chen, H.; Qiu, C.; Kwok, H. S.; Zhan, X.; Liu, Y.; Zhu, D.; Tang, B. Z. Aggregation-Induced Emission of 1-methyl-1,2,3,4,5-pentaphenylsilole. *Chem. Commun.* **2001**, 1740−1741.
(40) Mei, J.; Leung, N. L. C.; Kwok, R. T. K.; Lam, J. W. Y.; Tang, B. Z. Aggregation-Induced Emission: Together We Shine, United We Soar! *Chem. Rev.* **2015**, *115*, 11718−11940.
(41) Kwok, R. T. K.; Leung, C. W. T.; Lam, J. W. Y.; Tang, B. Z. Biosensing by Luminogens with Aggregation Induced Emission Characteristics. *Chem. Soc. Rev.* **2015**, *44*, 4228−4238.
(42) Shi, H. B.; Kwok, R. T. K.; Liu, J. Z.; Xing, B. G.; Tang, B. Z.; Liu, B. Real-Time Monitoring of Cell Apoptosis and Drug Screening Using Fluorescent Light-Up Probe with Aggregation-Induced Emission Characteristics. *J. Am. Chem. Soc.* **2012**, *134*, 17972−17981.
(43) Shi, H. B.; Liu, J. Z.; Geng, J. L.; Tang, B. Z.; Liu, B. Specific Detection of Integrin $\alpha_v\beta_3$ by Light-Up Bioprobe with Aggregation Induced Emission Characteristics. *J. Am. Chem. Soc.* **2012**, *134*, 9569−9572.
(44) Yuan, Y.; Xu, S.; Cheng, X.; Cai, X.; Liu, B. Bioorthogonal Turn-On Probe Based on Aggregation-Induced Emission Characteristics for Cancer Cell Imaging and Ablation. *Angew. Chem., Int. Ed.* **2016**, *55*, 6457−6461.
(45) He, X.; Zhao, Z.; Xiong, L.-H.; Gao, P. F.; Peng, C.; Li, R. S.; Xiong, Y.; Li, Z.; Sung, H. H.-Y.; Williams, I. D.; Kwok, R. T. K.; Lam, J. W. Y.; Huang, C. Z.; Ma, N.; Tang, B. Z. Redox-Active AIEgen Derived Plasmonic and Fluorescent Core@shell Nanoparticles for Multimodality Bioimaging. *J. Am. Chem. Soc.* **2018**, *140*, 6904−6911.
(46) Wang, J.-J.; Jiang, Y.; Lin, Y.; Wen, L.; Lv, C.; Zhang, Z.; Chen, G.; Pang, D.-W. Simultaneous Point-of-Care Detection of Enterovirus 71 and Coxsackievirus B3. *Anal. Chem.* **2015**, *87*, 11105−11112.
(47) Hu, J.; Jiang, Y.; Wu, L.; Wu, Z.; Bi, Y.; Wong, G.; Qiu, X.; Chen, J.; Pang, D.-W.; Zhang, Z.-L. Dual-Signal Readout Nanospheres for Rapid Point-of-Care Detection of Ebola Virus Glycoprotein. *Anal. Chem.* **2017**, *89*, 13105−13111.
(48) Draz, M.; Lakshminaraasimulu, N.; Krishnakumar, S.; Battalapalli, D.; Vasan, A.; Kanakasabapathy, M.; Sreeram, A.; Kallakuri, S.; Thirumalaraju, P.; Li, Y.; Hua, S.; Yu, X.; Kuritzkes, D.; Shafiee, H. Motion-Based Immunological Detection of Zika Virus Using Pt-Nanomotors and a Cellphone. *ACS Nano* **2018**, *12*, 5709−5718.

DOI: 10.1021/acsnano.8b05270
ACS Nano 2018, 12, 9549−9557